REGIONAL PHASE AMPLITUDE TOMOGRAPHY FOR SEISMIC VERIFICATION IN CHINA

W.S. Phillips, H.E. Hartse, S.R. Taylor, A.A. Velasco and G.E. Randall
Seismic Research Center, Los Alamos National Laboratory, Los Alamos, New Mexico

Sponsored by U.S. Department of Energy
Office of Nonproliferation and National Security
Office of Research and Development
Contract No. W-7405-ENG-36

ABSTRACT

We have applied tomographic techniques to amplitude data to quantify regional phase path effects for use in source discrimination and magnitude studies. Advantages of tomography over interpolation (kriging) methods of path correction include extrapolation into inactive regions, as well as increased levels of confidence in the resulting path corrections because of their more physical basis. Disadvantages include the smoothing inherent to tomography, which yields poorer fit to data; however, this can be overcome by incorporating interpolated residuals into the final correction surfaces for use in routine monitoring. Our tomography technique solves for resolvable combinations of attenuation, source-generation, site and spreading terms. First difference regularization is used to remove singularities and reduce noise effects.

In initial tests, the technique was applied to a data set of 1488, 1.0 Hz, P_g/L_g amplitude ratios from 13 stations for paths inside a 30° by 40° box covering western China and surrounding regions. Tomography reduced variance 60%, relative to the power law correction traditionally applied to amplitude ratios. Relative P_g/L_g attenuation varied with geologic region, with low values in Tibet, intermediate in basins and high for platforms and older crust. Comparing with results of prior path effect studies in this region, spatial patterns were most consistent with local earthquake coda-Q of Jin and Aki (1988). Relative spreading was consistent with expected values for P_g and L_g. Relative site terms were similar to one another, yet some tradeoff with attenuation was evident.

Examination of the tomography residuals using a kriging interpolator showed coherent geographical variations, indicating unmodeled path effects. The residual patterns often follow geological boundaries, which could result from attenuating zones or blockages that are too thin to be resolved, or that have anisotropic effect on regional phases. These results will guide efforts to reparameterize tomography models to more effectively represent regional wave attenuation and blockage. Future work will also test combining regionally varying attenuation with source parameter inversion (magnitude-distance amplitude correction, or MDAC; Taylor et al., 1999).

Key Words: Tomography, attenuation, discrimination, regionalization.

OBJECTIVE

Removing the effect of propagation path on regional seismic wave amplitudes is important for isolating source effects and will lead to more effective discrimination between natural and man-made seismic events. This is a crucial effort for extending verification monitoring techniques to small events. Here, we investigate the use of tomographic imaging to obtain amplitude path corrections for use in event discrimination and magnitude determination at regional distances.

RESEARCH ACCOMPLISHED

Background

The quantification of path effects on regional phase amplitudes has received much attention of late. Interpolation has been shown to be the most effective method, in terms of reducing variance in amplitude data (Phillips et al, 1997; Taylor and Hartse, 1998; Phillips et al., 1998; Phillips, 1999; Rodgers et al., 1999). These studies show that interpolated surfaces correlate well with regional geology; thus they reflect path, rather than coherent source radiation effects. Although earlier work was performed with simple, moving window smoothers, we currently prefer the Bayesian kriging interpolator of Schultz et al., (1998). Kriging provides error estimates and continuously differentiable surfaces, while the Bayesian modifications control extrapolation of the surface and errors into regions devoid of calibration events. This allows the inclusion of background models by kriging the model residuals and merging the results with a map of the model predictions.

Models based on correlations of amplitude data with physical data such as topography, basin thickness and moho depth can be used to predict path effects (e.g. Zhang and Lay, 1994; Fan and Lay, 1998). Such models are less effective than interpolation methods in reducing variance in amplitude data (Phillips, 1999; Rodgers et al., 1999), but have the advantage of extrapolating path effects beyond regions where data exist. Phillips (1999) demonstrated the effectiveness of combining the two methods by applying Bayesian kriging interpolation to the model residuals.

Tomographic images of the attenuation of regional phases can also be used to predict path effects (e.g. Singh and Hermann, 1983; Campillo, 1987; Xie and Mitchell, 1990; Campillo et al., 1993; Mitchell et al., 1997; Sandvol et al., 1998). Tomography complements interpolation methods because images can be well resolved in areas where no events occur. In addition, the physical basis of tomography increases our confidence in the derived path corrections. In this study, we test tomography techniques using regional phase amplitude data, with emphasis on the use of results in an automatic monitoring scheme.

In initial tests, we applied tomography techniques to 1 Hz P_g/L_g amplitude ratio data. We chose to start with ratio data because cross-phase relative source and site effects tend to be less dependent on source size, while relative path effects still exhibit large regional variation. This decreases the influence of a possibly error prone m_b that is used to correct for source size and scaling prior to inversion. Of course, using ratios will lead to difficulties in interpreting results because two phases are involved. In addition, monitoring would require a correction surface for every ratio that might be desired, which is a large number if we consider all bands and phases that can be observed. For these reasons, we support the use of single phase correction surfaces for routine monitoring and plan to test single phase tomography in the future.

We have chosen to analyze 1 Hz data in our initial tests. This band is useful for technique development because it offers the most data and coverage; however, 1 Hz ratios perform relatively poorly in discrimination (Walter et al., 1995; Taylor, 1996; Hartse et al., 1997). Results in this band can still be useful for magnitude estimation or for defining geophysically distinct regions that will be useful for assessing performance capabilities. Furthermore, low frequency data can improve the performance of multivariate discriminants (Taylor and Hartse, 1997). As we move to higher frequencies, our hope is that path corrections will lower the frequency threshold at which source types are observed to separate (3 to 4 Hz), allowing the inclusion of smaller and more distant events that might be of poor signal-to-noise in the most effective discriminant bands (6-8 Hz).

In the following, we will outline data reduction procedures for stations in China and surrounding regions, and describe the tomographic method we applied. We will show relative attenuation results that correlate well with geological province as well as spatially coherent, unmodeled data that suggest new avenues of development.

Data

We used the Preliminary Determination of Epicenters (PDE) catalog to guide the collection of regional event data from 13 broadband stations in China and surrounding regions archived at the Incorporated Research Institutions for Seismology, Data Management Center. We retrieved data from all possible, regional distance PDE events occurring between 1986 and 1996 from the now Global Seismic Network stations in China: Enshi (ENH), Lhasa (LSA), Lanzhou (LZH), Urumchi (WMQ) and Xian (XAN), as well as Boravoye (BRVK), Kurchatov (KURK) and Makanchi (MAK) in Kazakhstan; Ala-Archa (AAK), Kirghizstan; Talaya (TLY) and Zalesovo (ZAL), Russia; Nilore (NIL) Pakistan; and Ulan Bator (ULN), Mongolia.

To process the data, we first determined arrival times of the regional phases manually. After correcting for the instrument, RMS amplitudes were obtained for a number of pass bands between 0.5 and 8 Hz using time-domain filtering techniques, aligning windows on picked arrivals if they existed or on preset group velocities if not (Hartse et al., 1997). We use vertical component, P_g/L_g ratios in the band 0.5 to 1 Hz in this study. The preset L_g group-velocity window was 3.6 to 3.0 km/s and the P_g group-velocity window was 6.2 to 5.2 km/s. Requiring paths to lie within a box defined by longitudes 70° to 110° and latitudes 25° to 55°, as well as distances between 300 and 2500 km, event depths less than 50 km and signal-to-noise (pre-Pn) greater than 2 for both phases, reduced the data set to 1488 records. A plot of the raypath distribution shows good coverage over most of the region (Figure 1).

Tomography Method

We solve for resolvable combinations of relative attenuation, site and spreading effects on regional phase amplitude ratios. For a homogeneous propagation model, we express RMS amplitude for a given frequency band,

$$a_{ijk} = c_k \; f(m_b^{\,i}) \; s_{jk} \; x_{ij}^{-\beta_k} \; e^{-\alpha_k x_{ij}},$$

where the i, j, k indices represent source, site and phase type, respectively, c_k is a source generation term, f is source scaling, taken as a known function of m_b (Cong et al., 1996; equations 6 and 10), s_j is site effect, x_{ij} is distance, β_k is the spreading coefficient and α_k is the spatial attenuation coefficient. We define a source-corrected amplitude,

$$D_{ijk} = \log_{10} a_{ijk} - \log_{10} f(m_b^{\,i}).$$

Taking logarithms gives,

$$D_{ijk} = \log_{10} c_k + \log_{10} s_{jk} - \beta_k \log_{10} x_{ij} - \alpha_k x_{ij} \log_{10} e.$$

We now discretize attenuation into an array of latitude-longitude centered ellipses of constant α, setting major and minor axes to $\sqrt{2}/2$ of the local grid spacing so ellipses centered on a box of four adjacent grid points meet at a single point in the center. Assuming a great circle path, we take the chord length across each ellipse it intersects and normalize by the total path length in degrees. Thus $\alpha_k x_{ij}$ becomes a sum of products of discretized α_k and normalized ellipse chords. Substituting capital letters for $\log_{10}$, we obtain,

$$D_{ijk} = C_k + S_{jk} - \beta_k X_{ij} - \log_{10} e \, \Sigma m \, \alpha_{km} \, \delta x_{ijm}, \qquad 1.$$

where the new index, m, represents the discretization of the attenuation model and the δx_{ijm} are the normalized ellipse-chord lengths. After taking phase ratios, relative generation, site, spreading and attenuation terms replace those of equation 1,

$$\Delta D_{ij} = \Delta C + \Delta S_j - \Delta\beta \, X_{ij} - \log_{10} e \, \Sigma_m \, \Delta\alpha_m \, \delta x_{ijm}. \qquad 2.$$

Tomographic inversion can be based on these linear equations once we rationalize singularities or tradeoffs between unknown parameters.

We use standard, least squares techniques to solve equations 1 or 2, which can be written in matrix form

$$Ax = d,$$

where d is the data vector, x is the vector of unknowns and A represents the model equations. We apply first difference regularization to reduce the influence of noise on the results and eliminate singularities due to unresolved combinations of model parameters. Second difference regularization is often used in tomographic studies, but the first difference is more powerful in resolving singularities (e.g. Phillips and Fehler, 1991). The least square solution is written,

$$x = (A^tW^tWA + S^t\Lambda^2S)^{-1}\ A^tW^td, \qquad 3.$$

where S represents the regularization equations, Λ is a diagonal matrix containing regularization weights, W is a diagonal matrix representing weights based on estimated data error and superscript t represents the transpose. Resolution and covariance are calculated via,

$$R = (A^tW^tWA + S^t\Lambda\text{-}S)^{-1}\ A^tW^tWA,$$
$$C = (A^tW^tWA + S^t\Lambda\text{-}S)^{-1}.$$

We can also estimate predicted data variance along a new path, which will be useful for creating correction surfaces,

$$\sigma_p^{\,2} = a^t\ C\ a,$$

where a is a column vector representing equation 1 or 2 for the new path, similar to a row of A (e.g. Draper and Smith, 1981).

The tomographic calculations have been implemented using a Jacobi conjugate gradient solver (ITPACK). We add switches that eliminate or combine unknown terms in equations 1 and 2 to avoid singularities. For example, the generation term must be combined with the site terms because neither can be resolved uniquely. More subtle tradeoffs can be evaluated by examining the resolution matrix.

We use residual variance to evaluate goodness of fit and model improvement. The trace of the resolution matrix is taken as the number of free parameters in the model (Tarantola, 1987), which is needed to calculate variance. Variance reduction will be quoted relative to a power-law fit with distance, which is the traditional correction for amplitude ratios in discrimination studies (e.g. Hartse et al., 1997).

Results

To parameterize the inversion, we examine residual variance for a range of discretization intervals and regularization parameters. For this study, 1° and 2° attenuation term grids allowed similar fits to data, while a 5° grid was too coarse to fit the data well. Results employing a grid spacing of 2° will be presented here. Regularization parameters must be chosen large enough to control the effects of noise, yet lie below the point where excessive smoothing causes the residual variance to increase rapidly (e.g. Phillips and Fehler, 1991). Our choice of 2.5 for attenuation regularization allowed 58 free parameters in the 2° model, as estimated from the trace of the attenuation portion of the resolution matrix. This number of free parameters is similar to that obtainable with an unregularized 5° grid; however, the finer grid allows more spatial freedom to fit the data. Holding attenuation regularization fixed, the site term regularization parameter was determined to be 0.5, following the same procedure. This regularization constrains poorly resolved site terms to be similar to well resolved site terms and helps to avoid tradeoffs between site and near-station attenuation terms.

We found the standard deviation of residuals after removing a power-law fit with distance to be 0.36, representing the initial scatter in the ratio data. Allowing attenuation, spreading and source generation terms free produced a residual standard deviation of 0.23, or a variance reduction of 59% relative to the power-law fit. Replacing the source generation term with individual site terms resulted in only slight improvement and a variance reduction just over 60%. We plot relative P_g/L_g attenuation, $\Delta\alpha_m$, in grayscale (Figure 2). As the equations are set up, positive $\Delta\alpha_m$ (light gray) indicate P_g attenuates faster than L_g, while negative $\Delta\alpha_m$ (dark gray) indicate the opposite. Color versions of the tomography results, superposed on a topography map for

interpretation purposes, can be found in Phillips et al. (1999). Only well-resolved portions of the image are plotted in Figure 2. Boundaries were placed at the 0.5 contour representing diagonal elements of the resolution matrix, after normalizing by the ratio of the number of grid points to free parameters in the attenuation model. The normalization adjusts for regularization effects, which reduce resolution by smoothing adjacent model parameters.

We find that P_g/L_g attenuation correlates well with geological province. The lowest values (low P_g, high L_g attenuation) fall within the Tibetan plateau. This low is bounded sharply to the north, by the Qaidam basin, and to the east, by the Guangxi platform, associated with the Sichuan basin. Intermediate to low values can be seen in the Qilian Shan and western Tien Shan ranges, as well as the Tarim, Ordos and Junggar basins. Note the sharp transition between the Junggar basin area and the surrounding mountain ranges. Highest P_g/L_g attenuation is found in the stable, platform areas to the north and in the Guangxi platform to the east. Higher values are also found for trans-Himalaya paths to Lhasa (LSA), similar to patterns noted in spectral Q studies of regional phases recorded at LSA (Reese et al., 1998). We expected higher values in the vicinity of station ZAL in Russia; however, the weak L_g observed for paths through the Tien Shan and border ranges, relative to other paths through the northern area, is responsible for the observed pattern of low values.

Relative site terms vary from –0.8 to –0.3 for these data, most clustering about –0.5. The mean can be considered the relative source generation term, which is incorporated into the site terms in this inversion. Including these terms improves the fit to data only slightly, yet adds definition to the attenuation image as site effects are more appropriately accounted for. The similarity between most well resolved site terms may be an advantage of applying tomography to ratio data. However, outlier site terms for KURK (-0.8) and LSA (-0.3) appear to reflect the attenuation from nearby areas, even though these terms are reasonably well resolved.

The relative spreading coefficient, $\Delta\beta$, was estimated to be 0.54±0.11 (standard error). Again, the positive value indicates P_g spreads more quickly than L_g. If we assume L_g spreading is 0.83 (Nuttli, 1973; Campillo et al., 1984), our $\Delta\beta$ of 0.54 implies a P_g spreading coefficient of 1.37, reasonably consistent with a numerical modeling estimate of 1.5 (Campillo et al., 1984). Synthetic calculations generated using the inversion result and including similar levels of Gaussian noise resulted in correct recovery of the results, with some tradeoff evident between spreading and the range of attenuation terms. Based on 100 runs with different realizations of noise, the mean and standard deviation of $\Delta\beta$ was 0.50 ± 0.08.

Discussion

The tomography results are consistent with previous Eurasian path effect studies. If we interpret the variation of P_g/L_g attenuation primarily to be the result of L_g effects, we can qualitatively compare with studies of L_g and L_g coda. Rapine et al. (1997) described of L_g propagation in China, based on regional data from many stations. Most of China is described as efficient for L_g, while the Tibetan plateau is described as inefficient. The boundary between the propagation regions matches our tomographic result very well. We fail to see an extra-low zone along the Tibetan plateau edges, as suggested by McNamara et al (1996); however, the regularization constraints might have smoothed out such a pattern. Mitchell et al. (1997) produced a tomographic map of 1 Hz, L_g coda Q for Eurasia. This map is roughly consistent with ours, except for Mongolia, where we see efficient L_g (high P_g/L_g attenuation) and the L_g coda Q predicts inefficient L_g. However, the L_g coda-Q maps are of significantly larger scale and lower resolution than those presented here. Perhaps the best correspondence, in terms of resolution, is with results of a local earthquake, crustal coda-Q study (Jin and Aki, 1988). The coda-Q measurements are unevenly distributed through China; however, where coverage is dense, such as along the eastern boundary of the Tibetan plateau, the patterns are very similar to ours. This points out the value to discrimination research in performing coda-Q studies in regions of dense station coverage, with care taken to limit the coda lapse times so only crustal materials are sampled (Phillips et al., 1988).

To examine the geographical distribution of inconsistent data, we interpolate tomography residuals, one station at a time. Interpolation is performed with a Bayesian kriging algorithm (Schultz et al., 1998), using a data correlation function appropriate for L_g amplitudes in central China (Anderson and Phillips, 1998). For all stations, we see coherent geographical variations, indicating path effects that are inconsistent with the tomography result. For many stations, such as BRVK (Figure 3), we see residual patterns that follow boundaries between geological regions. For BRVK, a sudden increase in P_g/L_g ratios along the northwest edge of the Tarim basin may indicate a long, thin zone of high L_g attenuation, or a blockage. The high attenuation may be a structural or scattering, rather than an intrinsic, effect. (e.g. Baumgardt, 1990). The blockage may have greater effect on raypaths traveling across the structure than those traveling parallel to the structure. Sub-parallel

raypaths would tend to wash out the high attenuation zone during tomographic inversion. Our smoothing and coarse parameterization contribute to this effect.

CONCLUSIONS AND RECOMMENDATIONS

The inconsistent data patterns suggest directions for future modifications of the tomography methods. We can explore relaxation of regularization constraints in areas of well resolved, high gradients. We can also include anisotropic effects into the model parameterization, as has been done for velocity tomography (Mele et al., 1998), and which may help with blockages. Lateral refraction will also produce inconsistent data, which will be a limiting effect unless we wish to incorporate 2-dimensional effects in the forward model. More general improvement could come from the addition of constraints from censored data into the tomography, as well as realistic data covariance reflecting correlation between data from nearby events. Furthermore, better magnitude estimates will reduce noise introduced by source corrections and facilitate the use of phase amplitude data, rather than ratios. The magnitudes could be improved by accounting for censoring effects on teleseismic amplitudes (e.g. McLaughlin, 1988), or by using regional envelopes or coda (Aki, 1980; Mayeda, 1993). Tomography of phase amplitudes, as opposed to ratios, will be simpler to interpret and to implement into a monitoring scheme. Comparison with ratio tomography results will indicate how well source effects have been accounted for.

The tomographic results can be used to correct for path effects and reduce scatter in discrimination studies. For each station, amplitudes or amplitude ratios, along with errors, can be predicted over a surrounding grid. This grid can be used during the course of routine monitoring. In addition, the tomography can be employed as a background model, and corrections calculated by applying Bayesian kriging to the residuals (Figure 3) to form the final correction surface. The kriging can take the tomography prediction errors into account in creating the correction surface. The final result will reflect the tomography model in areas where events rarely occur and an interpolated version of the data in areas where events do occur.

REFERENCES

Aki, K. (1980). Physical basis for the duration magnitude and recommended practice for coda magnitude determination, *Proc. 17th Assemb. ESC*, Budapest, 73-77.

Anderson, K.K. and W.S. Phillips (1998). A simple procedure for kriging left-censored data, *EOS Trans. Am. Geophys. Union* **79**, F555.

Baumgardt, D. (1990). Investigation of teleseismic L_g blockage and scattering using regional arrays, *Bull. Seism. Soc. Am*. **80**, 2261-2281.

Campillo, M., M. Bouchon and B. Massinon (1984). Theoretical study of the excitation, spectral characteristics and geometrical attenuation of regional seismic phases, *Bull. Seism. Soc. Am*. **74**, 79-90.

Campillo, M. (1987). L_g wave propagation in a laterally varying crust and the distribution of the apparent quality factor in central France, *J. Geophys. Res.* **92**, 12604-12614.

Campillo, M., B. Feignier, M. Bouchon and N. Bethoux, Attenuation of crustal waves across the Alpine range, *J. Geophys. Res.* **98**, 1987-1996.

Cong, L.L, J.K. Xie and B.J. Mitchell (1996). Excitation and propagation of L_g from earthquakes in central Asia with implication for explosion/earthquake discrimination, *J. Geophys. Res*., **101**, 27779-27789.

Draper, N.R. and H. Smith (1981). *Applied Regression Analysis*, Second Edition, John Wiley & Sons, New York.

Fan, G. and T. Lay (1998). Statistical analysis of irregular waveguide influences on regional seismic discriminants in China, *Bull. Seism. Soc. Am*., **88**, 74-88.

Hartse, H.E., S.R. Taylor, W.S. Phillips and G.E. Randall (1997). A preliminary study of regional seismic discrimination in central Asia with emphasis on western China, *Bull. Seism. Soc. Am*., **87**, 551-568.

Jin, A. and K. Aki (1988). Spatial and temporal correlation between coda *Q* and seismicity in China, *Bull. Seism. Soc. Am*. **78**, 741-769.

McNamara, D.E., T.J. Owens and W.R. Walter (1996). Propagation characteristics of L_g across the Tibetan plateau, *Bull. Seism. Soc. Am*. **86**, 457-469.

Mayeda, K. (1993). $m_{bLgcoda}$: A stable single station estimator of magnitude, *Bull. Seism. Soc. Am*. **83**, 851-861.

McLaughlin, K.L. (1988). Maximum-likelihood event magnitude estimation with bootstrapping for uncertainty estimation, *Bull. Seism. Soc. Am*. **76**, 855-862.

Mele, G., A. Rovelli, D. Seber, T.M. Hearn and J. Barazangi (1998). Compressional velocity structure and anisotropy in the uppermost mantle beneath Italy and surrounding regions, *J. Geophys. Res*. **103**, 12529-12543.

Mitchell, B.J., Y. Pan, J. Xie and L. Cong (1997). L_g coda Q variation across Eurasia and its relation to crustal evolution, *J. Geophys. Res*. **102**, 22767-22779.

Nuttli, O.W. (1973). Seismic wave attenuation and magnitude relations for eastern North America, *J. Geophys. Res.* **78**, 876-855.

Phillips, W.S., W.H.K. Lee and J.T. Newberry (1988). Spatial variation of crustal coda Q in California, *Pure App. Geophys*. **128**, 251-260.

Phillips, W.S. and M.C. Fehler (1991). Traveltime tomography: A comparison of popular methods, *Geophysics* **56**, 1639-1649.

Phillips, W.S., G.E. Randall, H.E. Hartse, S.R. Taylor and H.J. Patton (1997). Source and path effects on regional phases in China, *Proc. 19th Ann. Seism. Res. Symp.* Orlando, 125-134.

Phillips, W.S., G.E. Randall and S.R. Taylor (1998). Path correction using interpolated amplitude residuals: An example from central China, *Geophys. Res. Lett.,* **25**, 2729-2732.

Phillips, W.S. (1999). Empirical path corrections for regional phase amplitudes, *Bull. Seism. Soc. Am*. **89**, 384-393.

Phillips, W.S., H.E. Hartse, S.R. Taylor, A.A. Velasco and G.E. Randall, Regional phase amplitude ratio tomography for seismic verification, submitted to Pure Appl. Geophys., 1999.

Rapine, R.R., J.F. Ni and T.M. Hearn (1997). Regional wave propagation in China and its surrounding regions, *Bull Seism. Soc. Am*., **87**, 1622-1636.

Reese, C.C., R.R. Rapine and J.F. Ni (1998). Lateral variation of Pn and L_g attenuation at the CDSN station LSA, *Bull. Seism. Soc. Am*. **88**, 325-330.

Rodgers, A.J., W.R. Walter, C. Schultz, S. Myers and T. Lay, (1999). A comparison of methodologies for representing path effects on regional P/S discriminants, *Bull. Seism. Soc. Am*., in press.

Sandvol, E., D. Seber, M. Barazangi, R. Mohamad, N. Turkelli, C. Gurbuz, E. Zor and R. Gok (1998). Seismological research in the Middle East, *Proc. 20th Ann. Seis. Res. Symp.* Santa Fe, 745-753.

Schultz, C., S. Myers, J. Hipp and C. Young (1998). Nonstationary Bayesian kriging: Application of spatial corrections to improve seismic detection, location and identification, *Bull. Seism. Soc. Am*. **88**, 1275-1288.

Singh, S. and R.B. Herrmann (1983). Regionalization of crustal coda-Q in the continental United States, *J. Geophys. Res.* **88**, 527-538.

Tarantola, A. (1987). *Inverse Problem Theory*, Elsevier, Amsterdam.

Taylor, S.R. (1996). Analysis of high-frequency P_g/L_g ratios from NTS explosions and western U.S. earthquakes, *Bull. Seism. Soc. Am*. **86**, 1042-1053.

Taylor, S.R. and H.E. Hartse (1997). An evaluation of generalized likelihood ratio outlier detection to identification of seismic events in western China, *Bull. Seism. Soc. Am*. **87**, 824-831.

Taylor, S.R. and H.E. Hartse (1998). A procedure for estimation of source and propagation amplitude corrections for regional seismic discriminants, *J. Geophys. Res*. **103**, 2781-2789.

Taylor, S.R., A.A. Velasco, H.E. Hartse, W.S. Phillips and W.R. Walter (1999), Amplitude corrections for regional seismic discriminants, submitted to *Pure Appl. Geophys*.

Walter, W.R., K.M. Mayeda and H.J. Patton (1995). Phase and spectral ratio discrimination between NTS earthquakes and explosions. Part I: Empirical observations, *Bull. Seism. Soc. Am*. **85**, 1050-1067.

Xie, J.K. and B.J. Mitchell (1990). A back-projection method for imaging large-scale lateral variations of L_g coda Q with application to continental Africa, *Geophys. J. Int*. **100**, 161-181.

Zhang, T.R. and T. Lay (1994). Analysis of short-period regional phase path effects associated with topography in Eurasia, *Bull. Seism. Soc. Am*., **84**, 119-132.

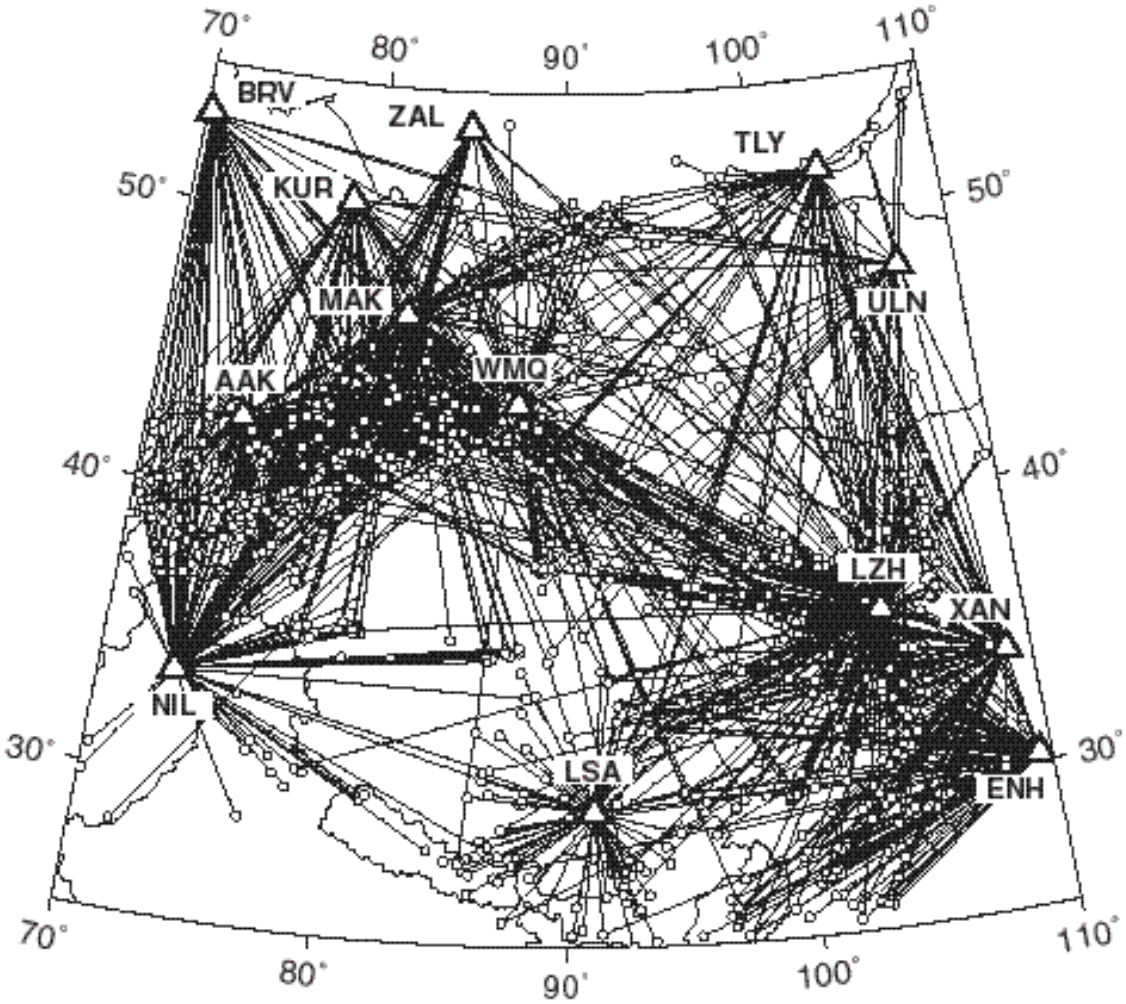

Figure 1. Great circle raypaths representing data used in tomographic inversion. Stations are indicated by triangles and events by circles.

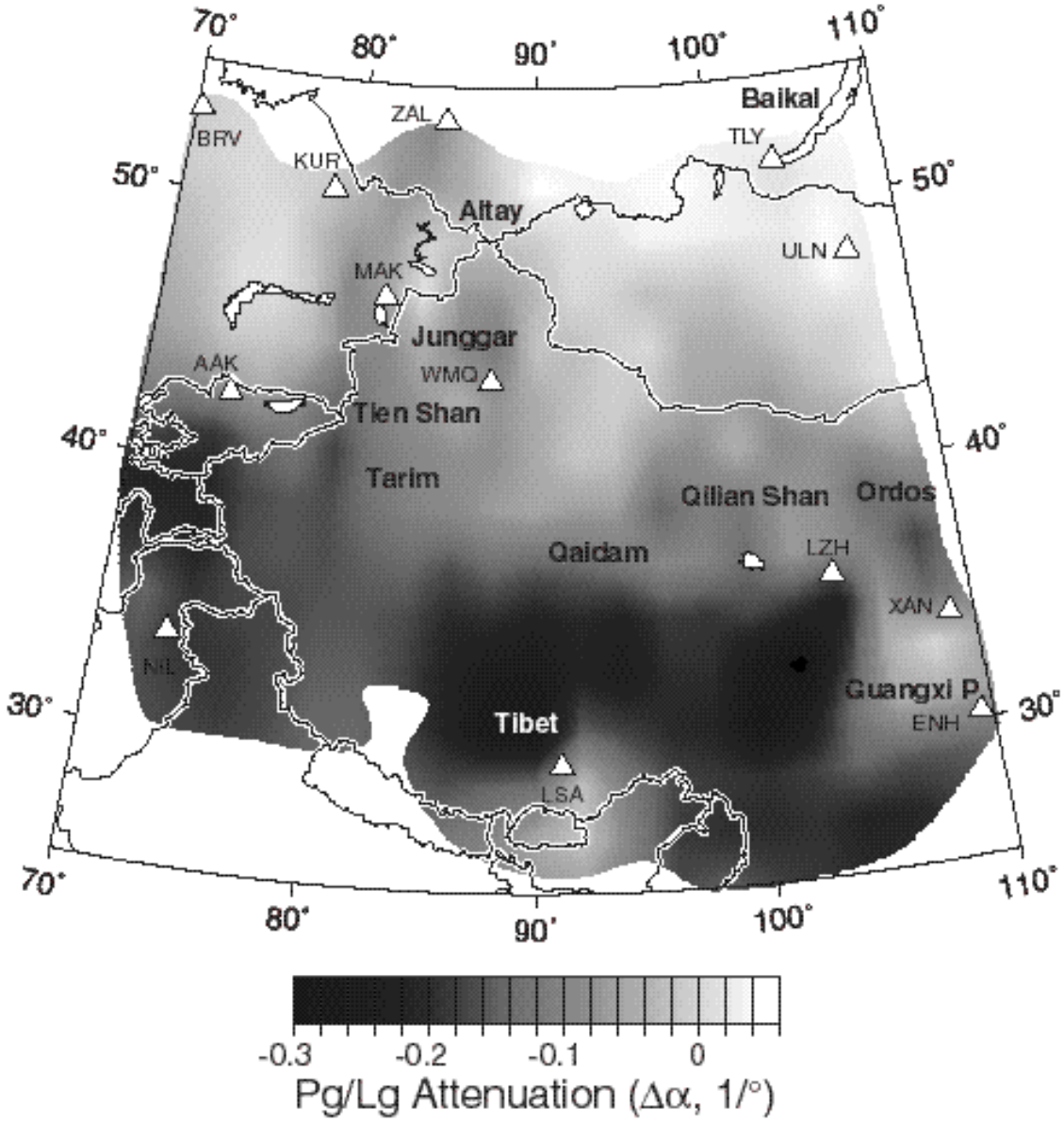

Figure 2. Relative attenuation from tomographic inversion of 1 Hz, P_g/L_g ratios. Light gray represents high relative attenuation (P_g attenuation high; L_g, low); dark gray, vice-versa. Only highly resolved portions of the image are shown. Annotations mark geographical and geological features mentioned in the text. Triangles represent stations that provided data for this study. Color facilitates the interpretation of these results and can be found in Phillips et al. (1999).

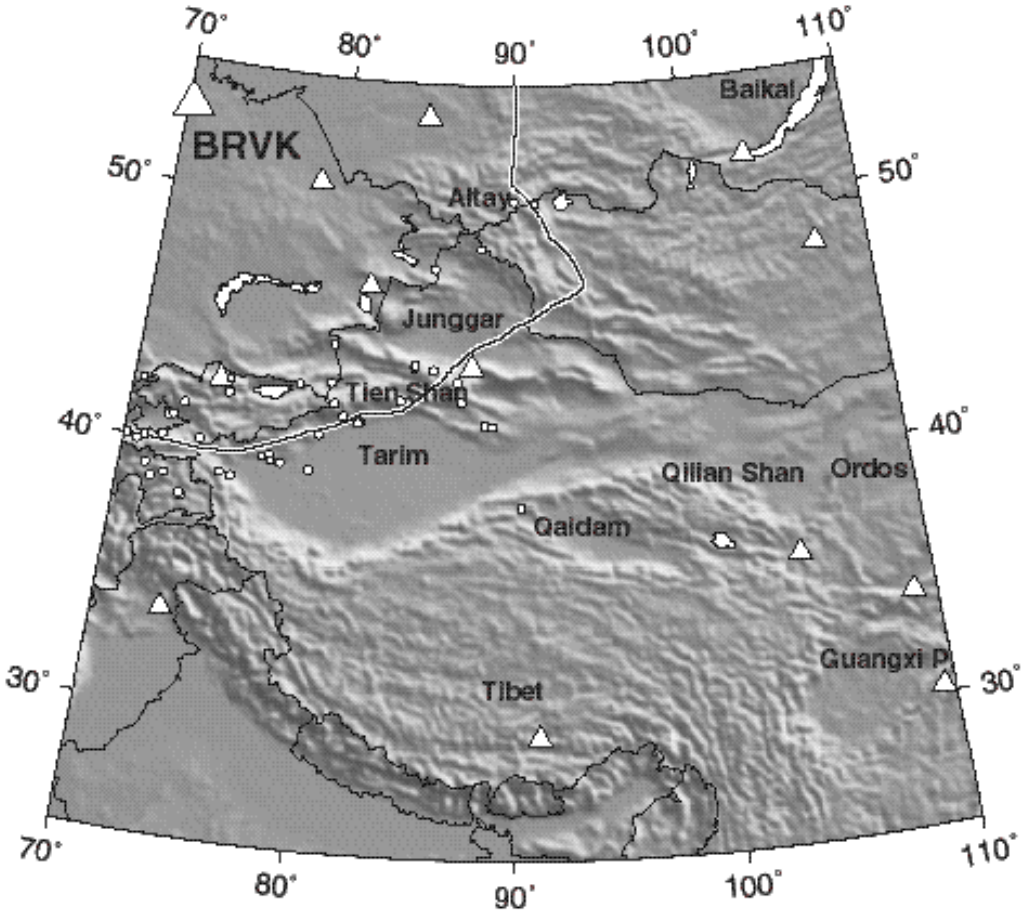

Figure 3. The zero contour of spatially interpolated $\log_{10} P_g/L_g$ residuals (data minus prediction) from station BRVK obtained by kriging (black on white line). Note the well-constrained portion of the contour that parallels the northwest edge of the Tarim basin. Underpredicted values fall to the south and east, overpredicted values to the north and west. Underpredicted data seek lower relative attenuation (darker gray, Figure 1) along their paths through the tomography image, overpredicted data, the opposite. Triangles represent stations providing data for the study.